Joint Probability Density Prediction for Multiperiod Thermal Ratings of Overhead Conductors

Xu Jin, Mengxia Wang, *Member*, *IEEE*, Mingjian Cui, *Senior Member*, *IEEE*, Hua Sun and Ming Yang, *Senior Member*, *IEEE*

Abstract—For an overhead conductor, meteorological correlations exist among the meteorological elements that dominantly determine its thermal rating, and temporal correlations exist among the thermal ratings in sequential time periods. It is necessary to exploit these correlations to improve the performance of the probabilistic prediction of thermal ratings. To this end, a copula-based method of joint probability density prediction for multiperiod thermal ratings (JPDP-MPTR) is presented in this paper. In this method, the probability density functions (PDFs) of the thermal ratings for every 15 minutes over a 1-hour horizon are first predicted individually, considering the correlations among meteorological elements. Then, the joint probability density function (JPDF) of the multiperiod thermal ratings is further formulated based on copula theory. Finally, the probability distributions of the thermal ratings in the predicted time periods are estimated via joint sampling based on the JPDF. Numerical simulations based on actual meteorological data collected around an overhead conductor show that the proposed method can significantly improve prediction results through the integration of meteorological and temporal correlations into the probabilistic prediction of the thermal rating.

Index Terms—Copula theory, meteorological elements, overhead conductor, probabilistic prediction, thermal rating

I. INTRODUCTION

At present, fossil energy shortages and severe environmental pollution are promoting the rapid expansion of renewable energy power generation, which is aggravating the load on power grids [1], [2]. An insufficient transfer capability in power grids has become one of the most important factors hindering the economical operation of power systems and the accommodation of renewable energy [3]. In this situation, system operators are required to make full use of the transmission capacity of existing transmission components to alleviate the shortage of transfer capability.

For thermally limited overhead conductors, to ensure safe operation, their thermal ratings are traditionally calculated under suitably conservative weather assumptions that either are fixed or vary seasonally [4] (known as static thermal ratings (STRs)). Although the STR is convenient to use, it is highly conservative in

most instances [4], [5]. To capture the actual transfer capability of overhead conductors, the dynamic thermal rating (DTR) technique was proposed in 1977 [6]. The DTR of an overhead conductor is calculated based on meteorological conditions measured in real time around the conductor [7]. Thus, the DTR of a conductor is varying in time and is significantly higher than the STR most of the time [8], [9]. Field studies have shown that the application of the DTR technique has played an important role in improving renewable power integration [10] and saving investment in power grid construction [11], [12]. Currently, the DTR technique has been developed to enable comprehensive monitoring of the temperature, mechanical tension, sag and meteorological environment of an overhead conductor. By taking advantage of sufficient measured data, the operating state, thermal model parameters and thermal rating of an overhead conductor can be estimated more accurately [13].

To enable the integration of the DTR into power system control decisions and guide operators to fully exploit the transfer capabilities of transmission lines, studies on thermal rating prediction have been conducted based on the DTR technique. In [14], the principal component regression method was used to predict steady-state conductor temperatures over a 12-hour horizon based on numerical weather predictions (NWPs). Then, the thermal ratings over the prediction time horizon could be indirectly calculated by estimating the allowable current increment based on the predicted conductor temperatures. The authors of [15] used an integrated factorized Ornstein-Uhlenbeck model to predict thermal ratings over a 24-hour horizon. In [16], NWPs were coupled with a computational fluid dynamics model to predict the wind conditions around a conductor. Then, the thermal ratings over an 18-hour horizon were calculated based on the predicted wind conditions combined with the air temperature and solar radiation data provided by the NWPs. These previous studies focused on point prediction of the thermal rating. However, the thermal rating of an overhead conductor is challenging to be predicted accurately due to the strong volatility of meteorological conditions. Thus, it is necessary to develop probabilistic prediction methods to reflect the uncertainty of the thermal rating predictions. To this end, the authors of [17] used the expectation-maximization algorithm to predict the probability density functions (PDFs) of day-ahead meteorological elements with 15-minute time steps based on NWPs and historical meteorological data in the vicinity of a conductor. Then, the PDFs of the day-ahead thermal ratings were calculated using meteorological data sampled from the predicted PDFs of the meteorological elements. In [18], the probability distributions of meteorological elements over a half-hour horizon were predicted using a conditional heteroscedastic auto-regressive model based on historical meteorological data in the vicinity of a conductor. Then, the kernel density estimation method was used to estimate the probability distributions of the thermal ratings based on thermal rating samples generated in accordance with the predicted probability distributions of the meteorological elements. [19] and

X. Jin, M. Wang, M. Yang are with the Key Laboratory of Power System Intelligent Dispatch and Control Ministry of Education, Shandong University, Jinan, Shandong Province, 250061, China (e-mail: wangmx@sdu.edu.cn).

M. Cui is with the Department of Electrical and Computer Engineering, Southern Methodist University, Dallas, TX 75275, USA (email: mingjiancui@smu.edu).

H. Sun is with the Technician Department, Shandong Labour Vocational and Technical College, Jinan, Shandong Province, 250022, China (email: 22478249@qq.com).

[20] provided the prediction intervals of day-ahead thermal ratings using machine learning methods based on NWPs and historical meteorological data in the vicinity of a conductor. In [21], the quantile regression (QR) method was used to predict the quantiles of day-ahead thermal ratings. Then, a risk-averse selection method for the optimal quantile was developed. It should be noted that one prerequisite in these previous studies was that the critical span of the overhead line was first identified using a corresponding technique [22], [23], and the DTR technique was then applied to this critical span.

Previous studies on the probabilistic prediction of thermal ratings are capable of providing prediction intervals and probability distributions of the thermal ratings in future time periods. However, these probabilistic predictions were conducted individually for each time period, without considering the correlations among multiperiod thermal ratings; that is, in these studies, series of single-period probability predictions were actually conducted over the prediction horizon. This may lead to overly wide prediction interval of the thermal rating, which is not consistent with the actual variation feature of the thermal rating. Therefore, to improve the performance of probabilistic prediction using the correlations that exist among multiperiod thermal ratings, a copula-based method of joint probability density prediction for multiperiod thermal ratings (JPDP-MPTR) is presented in this paper. The main contributions of this paper are as follows:

1) Based on meteorological data measured around an overhead conductor, the correlations among the four meteorological elements and the correlations among multiperiod thermal ratings are analyzed and revealed.

2) A copula-based JPDP-MPTR method is proposed. In this method, the PDFs of the thermal ratings in future time periods are first predicted via a series of single-period probabilistic predictions. A probabilistic prediction method considering the correlations among the four meteorological elements is proposed for these single-period predictions. Subsequently, the joint probability density function (JPDF) of the multiperiod thermal ratings is formulated using a selected copula model.

The remainder of this paper is organized as follows. Section II introduces the method of calculating the thermal rating of an overhead conductor. Section III analyzes the correlations among meteorological elements and the correlations among multiperiod thermal ratings based on meteorological data measured around an overhead conductor. Section IV presents the proposed JPDP-MPTR method. Section V analyzes the prediction results of the proposed method, and conclusions are drawn in Section VI.

II. THERMAL RATING CALCULATION

According to the relevant IEEE standard [24], the steady-state heat balance equation for an overhead conductor can be expressed as

$$q_j\left(T_{avg}\right)+q_s = q_c\left(T_s\right)+q_r\left(T_s\right), \qquad (1)$$

where T_{avg} is the average conductor temperature (℃), T_s is the conductor surface temperature (℃), q_j is the Joule heat produced by the current per unit length of the conductor (W/m), q_s is the solar heat gain (W/m), q_c is the heat loss caused by convection (W/m), and q_r is the heat loss caused by the heat radiation (W/m). The calculation formulas for the heat gain and heat loss terms in (1) are given as follows:

$$q_j(T_{avg}) = I^2 R(T_{avg}), \qquad (2)$$

$$R(T_{avg}) = [\frac{R(T_{high})-R(T_{low})}{T_{high}-T_{low}}]\times(T_{avg}-T_{low})+R(T_{low}), \qquad (3)$$

$$q_s = \alpha_s Q_{se} \sin(\theta)A', \qquad (4)$$

$$\begin{cases} q_{c1} = [1.01+1.35(\frac{D\rho_f V_w}{u_f})^{0.52}]k_f k_{angle}(T_s-T_a) \\[2mm] q_{c2} = 0.754(\frac{D\rho_f V_w}{u_f})^{0.6} k_f k_{angle}(T_s-T_a) \\[2mm] q_{c3} = 3.645\rho_f^{0.5} D^{0.75}(T_s-T_a)^{1.25} \end{cases}, \qquad (5)$$

$$q_r(T_s) = 17.8D\varepsilon[(\frac{T_s+273}{100})^4-(\frac{T_a+273}{100})^4]. \qquad (6)$$

In (2), I is the current of the conductor (A), and $R(T_{avg})$ is the resistance per unit length of the conductor (Ω/m) at temperature T_{avg}. Equation (3) characterizes the resistance-temperature effect of the conductor, where [T_{low}, T_{high}] is the effective range of the linear resistance-temperature relationship; T_{low}=25 ℃ and T_{high}=75 ℃ are used in this paper. In (4), α_s is the solar absorptivity of the conductor, Q_{se} is the solar radiation per unit square area on the ground after elevation correction (W/m^2), θ is the angle of incidence of the sun's rays (°), and A' is the projection area per unit length of the conductor (m^2/m). In (5), D is the diameter of the conductor (m), ρ_f is the air density (kg/m^3), μ_f is the air viscosity (kg/m-s), V_w is the wind speed (m/s), and k_{angle} is a wind direction factor that is related to the angle between the wind direction and the conductor axis (φ). q_{c1} and q_{c2} are used to calculate the forced convection heat loss rates caused by a low wind speed and a high wind speed, respectively. Under a given wind speed, it is recommended to use the greater of q_{c1} and q_{c2}. q_{c3} is used to calculate the natural convective heat loss rates under zero wind speed. IEEE Standard 738 recommends that the larger value between the forced and natural convection heat loss rates should be used at low wind speeds. In (6), ε is the heat radiation coefficient of the conductor, and T_a is the ambient temperature around the conductor (℃).

As seen from (2)-(6), once the location and type of an overhead conductor have been determined, the thermal rating of the conductor mainly depends on four meteorological elements around the conductor: the ambient temperature (T_a), wind speed (V_w), wind direction (φ), and solar radiation (Q_{se}). Based on the given values of these meteorological elements, the thermal rating of an overhead conductor can be calculated as

$$I_{max} = \sqrt{\frac{q_c\left(T_{max}\right)+q_r\left(T_{max}\right)-q_s}{R\left(T_{max}\right)}}, \qquad (7)$$

where T_{max} is the maximum permissible temperature of the conductor and I_{max} is the thermal rating of the conductor; T_{avg} and T_s are assumed to be equal to T_{max} in the calculation of I_{max}.

For an operational overhead conductor, correlations exist among the four meteorological elements in its vicinity, referred to as meteorological correlations. For example, a positive correlation exists between solar radiation and air temperature. In addition, for each meteorological element, autocorrelation also exists within its time series, introducing temporal correlations among the multiperiod thermal ratings of the overhead conductor. In this paper, an attempt is made to integrate these meteorological and temporal correlations into the probabilistic prediction of the thermal rating to improve the predictive performance.

III. DATA ANALYSIS

In this section, historical data on the four meteorological elements around an overhead conductor are used to analyze the meteorological and temporal correlations.

We collected meteorological data around a 220 kV overhead conductor ACSR300/40 (the cross-sectional areas of the aluminum part and the steel core of the ACSR are 300 mm^2 and 40 mm^2, respectively) in 2018 for 8760 hours in total, with a 15-minute time resolution. Scatterplots of pairwise combinations of the ambient temperature, wind speed, and solar radiation are shown in Fig. 1. Rose diagrams of the wind direction and the other meteorological elements are shown in Fig. 2.
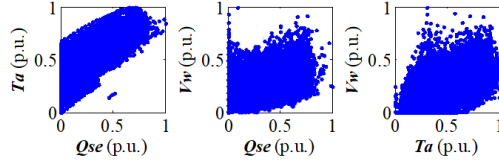
Fig. 1 Scatterplots of pairwise combinations of the ambient temperature, wind speed, and solar radiation.
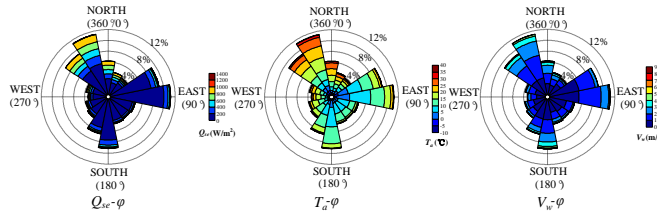
Fig. 2 Rose diagrams of the wind direction and the other meteorological elements.

According to the historical meteorological data, the correlation coefficients among the four meteorological elements are as shown in Table I.

TABLE I
CORRELATION COEFFICIENTS AMONG THE FOUR METEOROLOGICAL ELEMENTS

Number	Meteorological elements	Correlation coefficient
1	$Q_{se} - T_a$	0.72
2	$Q_{se} - V_w$	0.56
3	$T_a - V_w$	0.52
4	$V_w - \varphi$	0.36*
5	$T_a - \varphi$	0.32*
6	$Q_{se} - \varphi$	0.28*

* Since the wind direction is a circular variable, correlation coefficients No. 4-No. 6 were calculated using the linear-circular rank correlation coefficient calculation method presented in [25].

As shown in Table I, the correlation coefficients are all greater than 0.1, indicating the existence of correlations among the four meteorological elements [26], [27]. In particular, correlation coefficients No. 1-No. 3 are greater than 0.5, indicating relatively strong correlations among the solar radiation, air temperature and wind speed, whereas the correlations between the wind direction and the other meteorological elements are relatively small.

The historical thermal ratings of the conductor can be calculated based on these meteorological data using Eq. (7). The autocorrelation functions (ACFs) of the thermal ratings under different retardation time windows (0-48 hours with 15-minute time steps) are shown in Fig. 3.
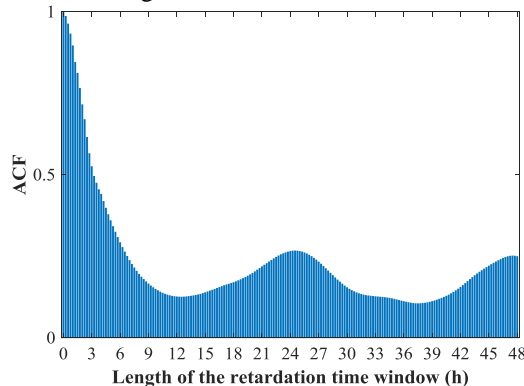
Fig. 3 ACFs under different retardation time windows.

As shown in Fig. 3, the ACFs of the thermal ratings under a retardation time window of up to 3 hours are greater than 0.5, indicating that the correlations among the multiperiod thermal ratings over a 3-hour horizon are relatively strong. In addition, the variation in the ACFs shows a diurnal periodicity.

Based on the above analysis, we set the length of the prediction time horizon to 1 hour. Then, 2-hour historical meteorological data were used to produce predictions of the thermal ratings with 15-minute time steps. A scatterplot matrix of the thermal ratings is presented in Fig. 4 to further illustrate the correlations among the thermal ratings in the four time periods over 1 hour.
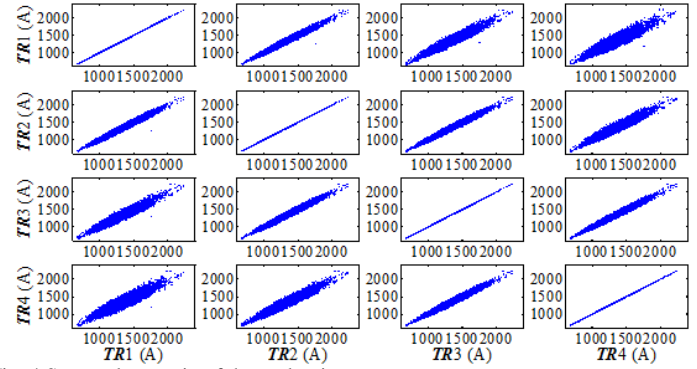
Fig. 4 Scatterplot matrix of thermal ratings.

In Fig. 4, $TR1$, $TR2$, $TR3$ and $TR4$ represent the thermal ratings in four time periods over 1 hour with 15-minute time steps. It can be seen from Fig. 4 that the distributions of the scattered points are almost concentrated into straight lines. This observation indicates that 1) strong positive correlations exist among $TR1$, $TR2$, $TR3$ and $TR4$ and 2) the distributions of the variations of thermal ratings among the different time periods are also highly concentrated. Fig. 5 shows the frequency distributions of the thermal rating variations over different time spans (15 minutes, 30 minutes, 45 minutes and 1 hour). Table II shows the 95% confidence intervals of the distributions of the thermal rating variations over different time spans.
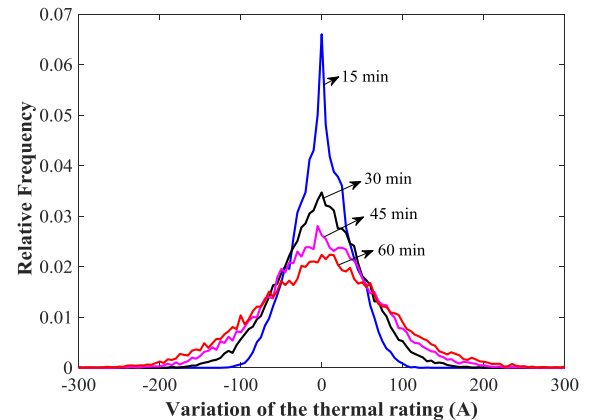
Fig. 5 Frequency distributions of the thermal rating variations over different time spans.

TABLE II
95% CONFIDENCE INTERVALS OF THE DISTRIBUTIONS OF THE THERMAL RATING VARIATIONS OVER DIFFERENT TIME SPANS

	Time span			
	15 min	30 min	45 min	1 hour
95% confidence interval	[-65A, 65A]	[-100A, 100A]	[-130A, 130A]	[-155A, 155A]

The above data analysis reveals the existence of correlations among the meteorological elements and among multiperiod thermal ratings. Perceptible correlations exist among some of the

meteorological elements. In addition, there are noticeable temporal correlations among the thermal ratings in the short term (1-3 hours).

IV. Copula-based JPDP-MPTR Method

To take advantage of meteorological and temporal correlations to improve the performance of probabilistic prediction, a copula-based JPDP-MPTR method is presented in this section.

In the developed method, a series of single-period probabilistic predictions are first carried out to predict the PDFs of the thermal ratings in future time periods over the prediction horizon. For each single-period prediction, a copula model is selected to generate the JPDF of the four meteorological elements to consider the meteorological correlations. Afterward, another copula model is selected to generate the JPDF of the multiperiod thermal ratings over the prediction horizon. The steps of the prediction process are presented in Subsection *A*. The technical details of the method for single-period probabilistic prediction are presented in Subsection *B*. Subsection *C* presents the JPDF prediction method for the multiperiod thermal ratings.

A. Prediction Process

A flowchart of the JPDP-MPTR method is shown in Fig. 6.
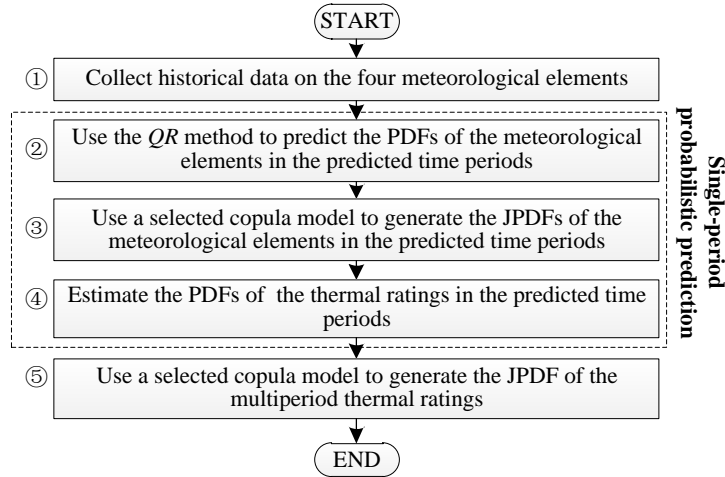
Fig. 6 Flowchart of the prediction process.

The prediction process is explained as follows:

1) In Step ①, meteorological data are collected around the target overhead conductor in preparation for prediction.

2) In Step ②, the *QR* method is used to predict the PDFs of the four meteorological elements in future time periods over the prediction horizon. The parameters of the *QR* models are trained using the collected meteorological data. Then, the quantiles of the four meteorological elements in the time periods of interest are predicted using the trained *QR* models. Subsequently, the PDFs of the meteorological elements in the predicted time periods over the prediction horizon can be obtained.

3) In Step ③, a copula model is selected to formulate the JPDFs of the four meteorological elements in the predicted time periods. Based on the formulated JPDFs, the four meteorological elements in each predicted time period can be jointly sampled. Then, the thermal ratings under the sampled groups of meteorological data (where one group consists of the values of the four meteorological elements) are calculated using Eq. (7). Subsequently, the PDF of the thermal rating in each predicted time period is estimated (see Step ④). By this means, the meteorological correlations are integrated into the single-period probabilistic predictions of the thermal ratings.

4) Finally, another copula model is selected to further formulate the JPDF of the multiperiod thermal ratings by treating the predicted PDFs of the thermal ratings in the predicted time periods as marginal PDFs (see Step ⑤).

B. Single-period Probabilistic Predictions of the Thermal Ratings in Future Time Periods

As mentioned above, the *QR* method is used to predict the probability distributions of the four meteorological elements (T_a, V_w, Q_{se}, and φ) in each predicted time period. For any one of T_a, V_w and Q_{se}, its τ quantile in the kth time period ($Q^k(\tau)$) of the prediction time horizon can be expressed by (8) in accordance with the linear *QR* model:

$$Q^k(\tau) = \beta_0^k(\tau) + \beta_1^k(\tau)x_1 + \beta_2^k(\tau)x_2 + \cdots + \beta_n^k(\tau)x_n , \; k=1\ldots m, \; (8)$$

where the x_i ($i=1\ldots n$) are the input parameters, namely, the historical data on the meteorological element; the $\beta_i^k(\tau)$ ($i=0\ldots n$; $k=1\ldots m$) are the regression parameters for the τ quantile of the meteorological element in the kth predicted time period; and m is the number of time periods over the prediction time horizon. In this paper, for each meteorological element, the historical 8-time-period data from the previous 2 hours are used as the input data for the *QR* model, and the length of the prediction time horizon is 1 hour, i.e., $n=8$ and $m=4$. The parameter vector $\boldsymbol{\beta^k}(\boldsymbol{\tau})$ can be estimated as follows:

$$\hat{\boldsymbol{\beta}}^k(\tau) = \arg\min_{\boldsymbol{\beta}^k \in \boldsymbol{R}} \sum_{i=1}^{n_{sz}} \eta_\tau^k \left(y_i - Q^k(\tau) \right) , \;\; k=1\ldots m, \quad (9)$$

where $\hat{\beta}^k(\tau)$ is the vector of the estimated regression parameters for the prediction of $Q^k(\tau)$, y_i is the actual meteorological element sample, n_{sz} is the sample size, and $\eta_\tau^k(\cdot)$ is a test function, which can be expressed as follows:

$$\eta_\tau^k(a) = \begin{cases} \tau \cdot a & a \geq 0 \\ (\tau-1) \cdot a & a < 0 \end{cases} , \;\; k=1\ldots m . \quad (10)$$

For the quantile prediction of the wind direction (φ) which is a circular variable, according to [18] and [28], before prediction, the wind direction can be decomposed along the easterly and northerly axes in the Cartesian coordinates into $\cos(\varphi)$ and $\sin(\varphi)$, respectively. Then, the *QR* model can be applied for the prediction of $\cos(\varphi)$ and $\sin(\varphi)$. The final wind direction prediction can then be obtained based on the prediction results of $\cos(\varphi)$ and $\sin(\varphi)$. Therefore, for wind direction prediction, the terms in (8) can be redefined as follows:

$$\boldsymbol{Q}^k(\tau) = \begin{bmatrix} Q_c^k(\tau) \\ Q_s^k(\tau) \end{bmatrix} \quad \boldsymbol{x}_i = \begin{bmatrix} x_{ci} \\ x_{si} \end{bmatrix} \\ \boldsymbol{\beta}_0^k(\tau) = \begin{bmatrix} \beta_{0c}^k(\tau) \\ \beta_{0s}^k(\tau) \end{bmatrix} \; \boldsymbol{\beta}_i^k(\tau) = \begin{bmatrix} \beta_{icc}^k(\tau) & \beta_{ics}^k(\tau) \\ \beta_{isc}^k(\tau) & \beta_{iss}^k(\tau) \end{bmatrix} , \quad (11)$$

where $Q_c^k(\tau)$ and $Q_s^k(\tau)$ are the τ quantiles of $\cos(\varphi)$ and $\sin(\varphi)$, respectively, in the kth time period and x_{ci} and x_{si} represent the historical data on $\cos(\varphi)$ and $\sin(\varphi)$, respectively. The parameter vectors $\boldsymbol{\beta}_c^k(\tau)$ and $\boldsymbol{\beta}_s^k(\tau)$ can be estimated as follows:

$$\begin{bmatrix} \hat{\boldsymbol{\beta}}_c^k(\tau) \\ \hat{\boldsymbol{\beta}}_s^k(\tau) \end{bmatrix} = \begin{bmatrix} \arg\min\limits_{\boldsymbol{\beta}_c^k \in \boldsymbol{R}} \sum_{i=1}^{n_{sz}} \eta_\tau^k \left(y_{ci} - Q_c^k(\tau) \right) \\ \arg\min\limits_{\boldsymbol{\beta}_s^k \in \boldsymbol{R}} \sum_{i=1}^{n_{sz}} \eta_\tau^k \left(y_{si} - Q_s^k(\tau) \right) \end{bmatrix} , \; k=1\ldots m , \; (12)$$

where $\hat{\boldsymbol{\beta}}_c^k(\boldsymbol{\tau})$ and $\hat{\boldsymbol{\beta}}_s^k(\boldsymbol{\tau})$ are the vectors of the estimated regression parameters for the prediction of $Q_c^k(\tau)$ and $Q_s^k(\tau)$, respectively, and y_{ci} and y_{si} are the actual $\cos(\varphi)$ and $\sin(\varphi)$ samples, respectively.

As shown in Fig. 7, $4 \times m$ *QR* models are trained to produce the single-period probabilistic predictions of the four meteorological elements in the predicted time periods.
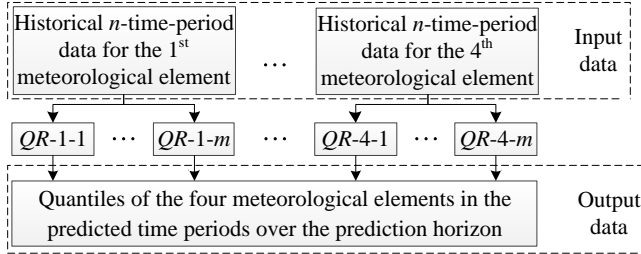
Fig. 7 Quantile prediction for the meteorological elements in the predicted time periods.

In Fig. 7, QR-i-k (i=1…4; k=1…m) represents the QR model for the ith meteorological element in the kth predicted time period. In this paper, the quantiles $Q^k(\tau)$ (τ=0, 0.01, 0.02, …,1) are predicted separately. The cumulative distribution functions (CDFs) and PDFs of the meteorological elements in the predicted time periods can be obtained by fitting the predicted quantiles.

A copula model is an effective tool for characterizing the correlations among multiple stochastic variables [29]. It can be used to formulate the JPDF of multiple stochastic variables. Suppose that there are z stochastic variables represented by r_1, r_2, …, r_z. According to copula theory, the joint CDF of these stochastic variables, $F(r_1,…,r_z)$, can be expressed as

$$F(r_1,\cdots,r_z) = C\big(F(r_1),\cdots,F(r_z)\big), \tag{13}$$

where $C(\cdot)$ is the copula distribution function and $F(r_1)$, …, $F(r_z)$ are the marginal CDFs of the stochastic variables. The JPDF of the stochastic variables, as shown in (14), can be derived by taking the derivative of (13) with respect to the stochastic variables on both sides:

$$f(r_1,\cdots,r_z) = c\big(F(r_1),\cdots,F(r_z)\big)\prod_{i=1}^{z} f(r_i), \tag{14}$$

where $c(\cdot)$ is the copula density function; $f(r_1,…,r_z)$ is the JPDF of the stochastic variables r_1, …, r_z; and the $f(r_i)$ (i=1…z) are the marginal PDFs of the stochastic variables r_1, …, r_z.

In the single-period predictions of the thermal ratings, for each predicted time period, the wind direction, wind speed, ambient temperature and solar radiation can be regarded as four stochastic variables, denoted by r_{w1}, r_{w2}, r_{w3}, and r_{w4}, respectively. Considering that the wind direction is a circular variable, a nonparametric Bernstein copula model is selected to predict the JPDFs of the four meteorological elements. According to [30] and [31], the quaternary empirical Bernstein copula density can be expressed as

$$c(u_{w1},u_{w2},u_{w3},u_{w4}) = \sum_{j_1=1}^{h}\sum_{j_2=1}^{h}\sum_{j_3=1}^{h}\sum_{j_4=1}^{h}\hat{p}_{j_1j_2j_3j_4}\prod_{l=1}^{4}\frac{(h)!}{(j_l-1)!(h-j_l)!}(u_{wl})^{j_l-1}(1-u_{wl})^{h-j_l}, \tag{15}$$

where $u_{wl}=F(r_{wl})$ (l=1,2,3,4), h is the order of the polynomial, and $\hat{p}_{j_1j_2j_3j_4}$ is given by

$$\hat{p}_{1j_2j_3j_4} = \hat{p}_{hj_2j_3j_4} = \frac{p_{1j_2j_3j_4}+p_{hj_2j_3j_4}}{2}, \tag{16}$$

$$\hat{p}_{j_1j_2j_3j_4} = p_{j_1j_2j_3j_4}, \quad j_1 \neq 1,h, \tag{17}$$

$$p_{j_1j_2j_3j_4} = \frac{1}{n_{sz}}\sum_{i=1}^{n_{sz}} I\left(\frac{j_1-1}{h} < u_{w1i} \leq \frac{j_1}{h},\frac{j_2-1}{h} < u_{w2i} \leq \frac{j_2}{h},\frac{j_3-1}{h} < u_{w3i} \leq \frac{j_3}{h},\frac{j_4-1}{h} < u_{w4i} \leq \frac{j_4}{h}\right), \tag{18}$$

where $I(\cdot)$ is an indicator function that takes a value of 1 when its argument is true and takes a value of 0 otherwise.

Based on the predicted PDFs of the four meteorological elements and the Bernstein copula density function, the JPDF of the four

meteorological elements in each predicted time period can be obtained. Then, the PDFs of the thermal ratings in the predicted time periods can be estimated using meteorological data sampled from the JPDFs of the four meteorological elements. In this paper, 2000 groups of meteorological data are sampled to simulate the PDF of the thermal rating in each predicted time period.

C. JPDF Prediction for Multiperiod Thermal Ratings

Once both the CDF and PDF of the thermal rating have been obtained for each predicted time period, as described in Subsection *B*, the thermal ratings in the four upcoming time periods over the prediction horizon can be regarded as four stochastic variables, r_{I1}, r_{I2}, r_{I3}, and r_{I4}. Since the thermal rating is a linear variable, for simplicity, a traditional parametric copula model can be used to predict the JPDF of the multiperiod thermal ratings. According to [31] and [32], there are multiple typical parametric copula models that can be used to characterize different correlation characteristics among stochastic variables, such as the Gaussian copula, the t-copula, the Clayton copula, the Frank copula and the Gumbel copula. Based on historical data on the stochastic variables, the Bayesian information criterion (BIC) can be used to select the optimal copula model [33]. The BIC for a copula model is computed as

$$BIC = -2\ln\big(L_m\big)+n_p\times\ln\big(n_s\big), \tag{19}$$

where L_m is the maximum value of the likelihood function for the JPDF formulated via the copula model based on the given samples, n_p is the number of parameters of the copula model, and n_s is the number of samples used for maximum likelihood estimation. In (19), the first term decreases with increasing L_m. Thus, a copula model with a smaller value of the first term is more suitable for formulating the JPDF of the stochastic variables. The second term reflects the complexity of the copula model. Its value increases with increasing model complexity. The second term functions as a penalty in the BIC calculation. Once the BICs for all candidate copula models have been calculated, the copula model with the minimum BIC will be selected as the optimal model because it is considered to provide the best tradeoff between model accuracy and complexity.

To select the optimal parametric copula model for the formulation of the JPDF of the multiperiod thermal ratings, the BICs for five candidate parametric copula models were calculated. The calculation results are given in Table III.

TABLE III
BICs OF CANDIDATE COPULA MODELS FOR THE FORMULATION OF THE JPDF OF THE MULTIPERIOD THERMAL RATINGS

Copula model	BIC
Gaussian copula	-25642.60
t-copula	**-30867.80**
Clayton copula	-27952.97
Frank copula	-29646.07
Gumbel copula	-28670.50

According to Table III, the t-copula model should be selected as the optimal parametric copula model for formulating the JPDF of the multiperiod thermal ratings. The quaternary t-copula density function is given by

$$c(u_{I1},u_{I2},u_{I3},u_{I4};\boldsymbol{\rho}_t,b)=\frac{|\boldsymbol{\rho}_t|^{-\frac{1}{2}}\Gamma\left(\frac{b+4}{2}\right)\left[\Gamma\left(\frac{b}{2}\right)\right]^3}{\left[\Gamma\left(\frac{b+1}{2}\right)\right]^4}\cdot\frac{\left(1+\frac{1}{b}\boldsymbol{\lambda}^T\boldsymbol{\rho}_t^{-1}\boldsymbol{\lambda}\right)^{-\frac{b+4}{2}}}{\prod_{i=1}^{4}\left(1+\frac{\left(t^{-1}(u_{Ii})\right)^2}{b}\right)^{-\frac{b+1}{2}}}, \tag{20}$$

where $u_{Ii}=F(r_{Ii})$ (i=1,2,3,4), $\boldsymbol{\lambda}^T=[t^{-1}(u_{I1}), …, t^{-1}(u_{I4})]$, $t^{-1}(\cdot)$ is the inverse CDF of the univariate t-distribution, $\Gamma(\cdot)$ represents the Γ distribution function, $\boldsymbol{\rho}_t$ is the 4th-order correlation coefficient matrix

of the 4-dimensional t-copula function, and b is the number of degrees of freedom. The parameters in $\boldsymbol{\rho}_t$ and the parameter b can be estimated using the maximum likelihood estimation method [34]. The likelihood function can be expressed as

$$L(\boldsymbol{\rho}_t,b)=\prod_{d=1}^{n_s}c(F(r_{I1d}),\cdots,F(r_{I4d});\boldsymbol{\rho}_t,b)f(r_{I1d})f(r_{I2d})f(r_{I3d})f(r_{I4d}), \quad (21)$$

where r_{I1d}, r_{I2d}, r_{I3d}, and r_{I4d} ($d=1, 2, \ldots, n_s$) denote the samples of the thermal ratings in the four time periods. Then, the parameters in $\boldsymbol{\rho}_t$ and the parameter b can be estimated as follows:

$$(\hat{\boldsymbol{\rho}}_t,\hat{b})=\arg\max\left(\ln L(\boldsymbol{\rho}_t,b)\right), \quad (22)$$

where $\hat{\boldsymbol{\rho}}_t$ is the estimated 4th-order correlation coefficient matrix of the 4-dimensional t-copula function and $\hat{b}$ is the estimated number of degrees of freedom. After parameter estimation, the t-copula density function and the PDFs of the thermal ratings in the four predicted time periods can be substituted into Eq. (14). Thus, the JPDF of the multiperiod thermal ratings can be obtained.

V. CASE STUDIES

In this case study, meteorological data were collected around an overhead conductor from July 1st, 2018, to August 14th, 2018 (45 days), with a 15-minute resolution (4320 groups of meteorological data in total). The type of overhead conductor used was ACSR 300. Its STR is 650 A, which is calculated under conservative weather conditions of an air temperature of 35 ℃, a wind speed of 0.5 m/s perpendicular to the conductor and a solar radiation level of 800 W/m². The first 30 days (2880 groups) of meteorological data were used as the training dataset to estimate the parameters of the *QR* model and the selected copula model. The remaining 15 days of data were used as the test dataset to verify the effectiveness of the proposed probabilistic prediction method. In this case study, the prediction horizon was taken to be 1 hour (consisting of four time periods for prediction). Accordingly, we conducted predictions hour by hour for a total of 15 days (360 hours).

A. Single-period Probabilistic Predictions of the Thermal Ratings in Future Time Periods

As described in Section IV, the *QR* method is first used to predict the marginal PDFs of the four meteorological elements in the upcoming time periods over the prediction horizon. Then, a nonparametric Bernstein copula model is used to formulate the JPDFs of the meteorological elements in these predicted time periods to consider the meteorological correlations. These JPDFs, as expressed in Eq. (23), are formulated by substituting the marginal PDFs and the Bernstein copula density function into Eq. (14):

$$f^k(r_{w1}^k,\cdots,r_{w4}^k)=\sum_{j_1=1}^{h}\sum_{j_2=1}^{h}\sum_{j_3=1}^{h}\sum_{j_4=1}^{h}\hat{p}_{j_1j_2j_3j_4}\prod_{l=1}^{4}\frac{(h)!}{(j_l-1)!(h-j_l)!}\left(u_{wl}^k\right)^{j_l-1}\left(1-u_{wl}^k\right)^{h-j_l}f^k(r_{wl}^k), \quad (23)$$

where r_{w1}^k, ..., r_{w4}^k are the stochastic variables representing the four meteorological elements in the kth predicted time period; $f^k(r_{w1}^k,\ldots,r_{w4}^k)$ ($k=1\ldots4$) denotes the JPDF in the kth predicted time period; the u_{wl}^k $=F^k(r_{wl}^k)$ ($l=1\ldots4$) denote the marginal CDFs of the stochastic variables r_{w1}^k, ..., r_{w4}^k in the kth predicted time period; and the $f^k(r_{wl}^k)$ ($l=1\ldots4$) are the marginal PDFs. According to [31] and [35], the order of the polynomial is $h=8$, which is chosen based on the quartic root of the sample size.

Based on Eq. (23), the four meteorological elements in each time period over the prediction horizon are jointly sampled. The thermal ratings in the predicted time periods are then calculated using Eq. (7) based on these meteorological samples. By statistics, the quantiles and PDFs of the thermal ratings in the predicted time periods can

then be obtained (hereafter called method I). In Fig. 8, the shaded area represents the area covered by the sampled thermal ratings (2,000 samples in each time step) drawn from the obtained PDFs. For comparison, single-period probabilistic predictions were also conducted using the predicted marginal PDFs of the four meteorological elements directly (hereafter called method II). The prediction process of method II is equivalent to the single-period probabilistic prediction process presented in Fig. 6 without Step ③. In addition, we attempted to produce probabilistic predictions using the historical thermal ratings (hereafter called method III). In method III, the historical thermal ratings are first calculated using the historical meteorological data. Corresponding *QR* models that take the historical thermal ratings as input are then trained to produce probabilistic predictions of the thermal ratings in the predicted time periods. The 0 quantiles and 1 quantiles predicted by methods II and III are also shown in Fig. 8 for comparison.
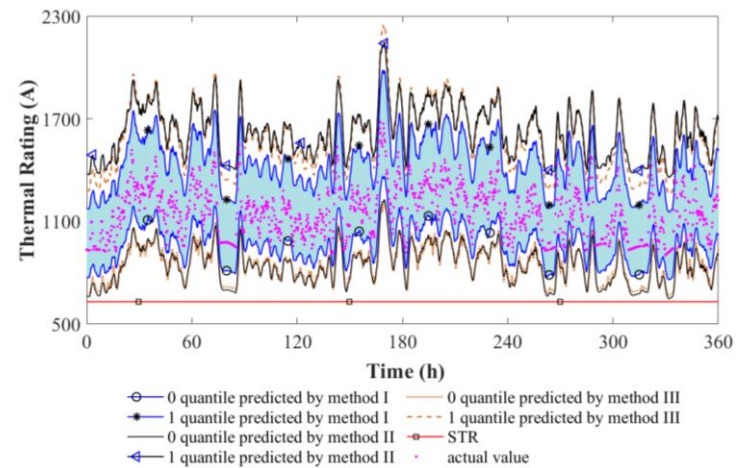
Fig. 8 Actual thermal ratings, STR, and prediction results of methods I, II and III.

It can be seen from Fig. 8 that all of the prediction intervals obtained using probabilistic prediction methods I, II and III fully cover the actual thermal rating curve. This indicates that all three methods achieve good performance in terms of reliability. However, the widths of the prediction intervals and the prediction accuracies of the three methods are different. Table IV shows the average widths of the prediction intervals (AWPIs), the mean absolute percentage errors (MAPEs) of the 0.5 quantiles of the prediction results relative to the actual thermal ratings, and the mean percentage deviations (MPDs) of the 0 quantiles relative to the STR. The MPD is calculated as follows:

$$MPD(\%)=Avg\left(\frac{(0\ quantile)-STR}{STR}\right)\times100 \quad (24)$$

Table IV shows that for the first three methods, the AWPI and the MAPE of the 0.5 quantile produced by method I are the smallest, followed by those of methods III and II, respectively. The predicted 0 quantile of the thermal rating is the most conservative choice for the system operator. Method I can produce the highest (least conservative) 0-quantile prediction result among the first three methods (approximately 116.94 A and 109.85 A higher on average than the prediction results of methods II and III, respectively), thereby guiding operators to make fuller use of overhead conductors. The above analyses illustrate that the integration of meteorological correlations into single-period probabilistic prediction is an effective way to improve the predictive performance.

B. Results of Multiperiod Joint Probabilistic Prediction

The selected t-copula model and the predicted marginal PDFs of the thermal ratings in the predicted time periods are substituted into Eq. (14) to formulate the JPDF of the multiperiod thermal ratings, which can be expressed as

$$f(r_{I1},\cdots,r_{I4}) = \frac{|\boldsymbol{\rho}_t|^{-\frac{1}{2}} \Gamma\left(\frac{b+4}{2}\right)\left[\Gamma(b)\right]^3}{\left[\Gamma\left(\frac{b+1}{2}\right)\right]^4} \frac{\left(1+\frac{1}{b}\boldsymbol{\lambda}^T \boldsymbol{\rho}_t^{-1}\boldsymbol{\lambda}\right)^{-\frac{b+4}{2}}}{\prod\limits_{i=1}^{4}\left(1+\frac{\left(t^{-1}(u_{Ii})\right)^2}{b}\right)^{-\frac{b+1}{2}}} \prod_{i=1}^{4} f(r_{Ii}), \quad (25)$$

where $f(r_{I1},\ldots,r_{I4})$ is the JPDF of the multiperiod thermal ratings, the $f(r_{Ii})$ $(i=1\ldots4)$ are the predicted marginal PDFs, and $\boldsymbol{\rho}_t$ and b can be estimated via maximum likelihood estimation based on the training dataset. After this estimation, we have $b=4$, and $\boldsymbol{\rho}_t$ is given as shown in (26):

$$\boldsymbol{\rho}_t = \begin{matrix} & TR1 & TR2 & TR3 & TR4 \\ \begin{pmatrix} 1 & 0.71 & 0.65 & 0.58 \\ 0.71 & 1 & 0.70 & 0.64 \\ 0.65 & 0.70 & 1 & 0.70 \\ 0.58 & 0.64 & 0.70 & 1 \end{pmatrix} & \begin{matrix} TR1 \\ TR2 \\ TR3 \\ TR4 \end{matrix} \end{matrix}. \quad (26)$$

It can be seen from (26) that over the 1-hour horizon, the correlation coefficient between the thermal ratings in two time periods decreases as the time span between them increases. Therefore, the estimation results for $\boldsymbol{\rho}_t$ reasonably reflect the degrees of correlation among the multiperiod thermal ratings.

By using Eq. (25), the thermal ratings in the four upcoming time periods over the prediction horizon can be jointly sampled. Accordingly, we sampled the thermal ratings hour by hour for a total of 15 days. The prediction results obtained using this method, hereafter called method IV, are shown in Fig. 9. The curves of the 0 and 1 quantiles predicted by method I are also shown in Fig. 9 for comparison.
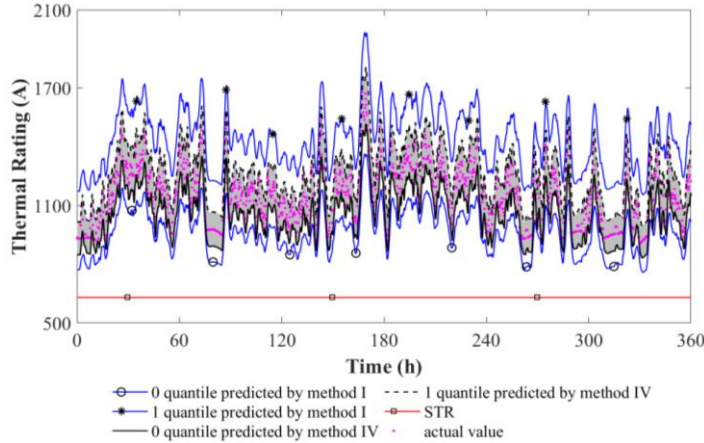
Fig. 9 Comparison of the multiperiod joint probabilistic prediction results and the single-period probabilistic prediction results from Subsection A.

TABLE IV
PARTIAL PREDICTION RESULTS OF PROBABILISTIC PREDICTION METHODS

	Probabilistic prediction method			
	I	II	III	IV
AWPI	466.75 A	774.34 A	746.65 A	202.18 A
MAPE of the 0.5 quantile	8.63%	18.68%	17.93%	5.65%
MPD of the 0 quantile	51.44%	33.45%	34.54%	66.08%

It can be seen from Fig. 9 that the prediction intervals obtained with the JPDP-MPTR method still fully cover the actual thermal rating curve while being narrower than those predicted by method I. According to Table IV, the JPDP-MPTR method (method IV)

produces the lowest AWPI and the lowest MAPE of the 0.5 quantile as well as the highest 0 quantile over the prediction time horizon. These findings illustrate that considering the temporal correlations among multiperiod thermal ratings can lead to prediction results that are more consistent with the actual characteristics of the thermal rating variations, thus further improving the probabilistic prediction performance.

C. Evaluation of the Probabilistic Predictions

For a probabilistic prediction method, the reliability and sharpness of the prediction results can be used to evaluate its performance [33].

Reliability refers to the ability of the prediction intervals to cover the actual values of the predicted variable. Specifically, the prediction interval coverage probability (PICP) should be close to the nominal confidence level $(1-\alpha)$. The PICP at the jth nominal confidence level $(PICP_j)$ can be defined as

$$PICP_j = \frac{1}{n_a}\sum_{i=1}^{n_a}\psi_{i,j}, \quad (27)$$

where n_a is the number of actual thermal ratings and $\Psi_{i,j}$ is the indicator for $PICP_j$, expressed as

$$\psi_{i,j} = \begin{cases} 1, & r_{ti} \in I_{i,j} \\ 0, & r_{ti} \notin I_{i,j} \end{cases}, \quad (28)$$

where r_{ti} is the ith actual thermal rating and $I_{i,j}$ is the ith prediction interval at the jth nominal confidence level. As mentioned above, the error between $PICP_j$ and $1-\alpha_j$ should be small, which means that the average coverage error (ACE), as defined in (29), should be as close to zero as possible. Therefore, the smaller the ACE is, the more reliable the prediction intervals.

$$ACE = \frac{1}{N}\sum_{j=1}^{N}\left|PICP_j - \left(1-\alpha_j\right)\right|. \quad (29)$$

In (29), N is the number of nominal confidence levels considered. In this case study, six different nominal confidence levels were selected $(1-\alpha_j=100\%, 98\%, 96\%, \ldots, 90\%)$.

Sharpness refers to the degree of concentration of the probability distributions. The interval score can be employed to reflect the sharpness of each individual prediction interval. The interval score of the ith prediction interval at the jth nominal confidence level, $Sc_{i,j}$, can be expressed as

$$Sc_{i,j} = \begin{cases} 2\alpha_j\left(U_{i,j}-L_{i,j}\right)+4\left(L_{i,j}-r_{ti}\right), & r_{ti} < L_{i,j} \\ 2\alpha_j\left(U_{i,j}-L_{i,j}\right), & r_{ti} \in I_{i,j} \\ 2\alpha_j\left(U_{i,j}-L_{i,j}\right)+4\left(r_{ti}-U_{i,j}\right), & r_{ti} > U_{i,j} \end{cases}, \quad (30)$$

where $U_{i,j}$ is the maximum value of the prediction interval and $L_{i,j}$ is the minimum value of the prediction interval. Based on $Sc_{i,j}$, the average score value (ASV) is defined as shown in (31) to reflect the overall sharpness of prediction intervals, where a smaller ASV indicates greater sharpness.

$$ASV = \frac{1}{Nn_a}\sum_{j=1}^{N}\sum_{i=1}^{n_a}Sc_{i,j}. \quad (31)$$

Based on (29) and (31), the ACEs and ASVs of the prediction results of the four probabilistic prediction methods were calculated, and the results are shown in Table V.

The continuous ranked probability score (CRPS) is a popular prediction evaluation criterion that can comprehensively reflect the reliability and sharpness of probabilistic prediction results. The CRPS has previously been applied to evaluate the performance of the thermal rating probabilistic prediction method [20]. The CRPS

for the thermal rating probabilistic prediction results can be expressed as

$$CRPS\left(f_i, r_{ti}\right) = \int_{-\infty}^{+\infty} \left(\int_{-\infty}^{r} f_i(x)dx - H\left(r - r_{ti}\right)\right)^2 dr \ , \quad (32)$$

where f_i is the PDF of the thermal rating in the ith predicted time period and $H(\cdot)$ is the Heaviside function, which is expressed as follows:

$$H(e) = \begin{cases} 0, & e < 0 \\ 1, & e \geq 0 \end{cases}. \quad (33)$$

It can be seen from (32) that when the prediction interval covers the actual thermal rating, the smaller the prediction interval is, the smaller the value of the CRPS. Therefore, a lower CRPS indicates better performance of a probabilistic prediction method. The 15-day CRPS curves of the four probabilistic prediction methods used in this paper are shown in Fig. 10. The average CRPSs of the four prediction methods are also shown in Table V.
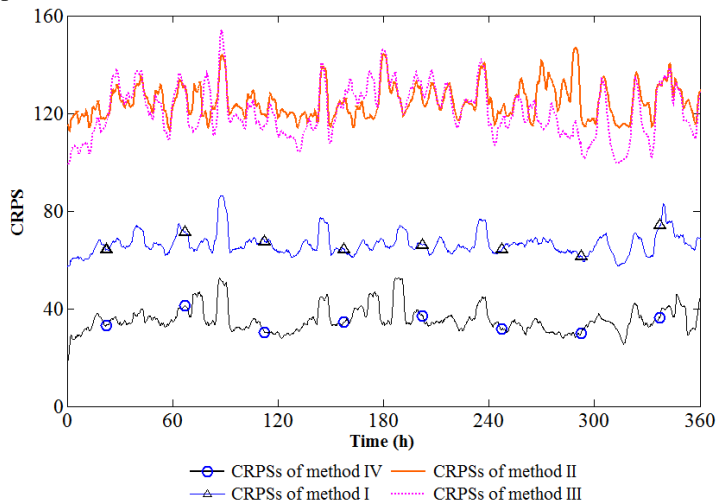
Fig. 10 CRPSs of the four probabilistic prediction methods.

TABLE V
ACEs, ASVs AND AVERAGE CRPSs OF THE FOUR PROBABILISTIC PREDICTION METHODS

	Probabilistic prediction method			
	I	II	III	IV
ACE	0.026	0.055	0.051	0.018
ASV	36.29	67.02	65.19	15.64
Average CRPS	70.54	125.18	122.86	38.96

As shown in Fig. 10 and Table V, method IV has the smallest ACE, ASV and average CRPS, followed by method I. This indicates that the proposed probabilistic prediction methods achieve better performance than the methods without considering meteorological correlations and temporal correlations among multiperiod thermal ratings.

VI. CONCLUSION

In this paper, a JPDP-MPTR method is proposed. The conclusions are as follows: 1) Correlations exist among meteorological elements and among multiperiod thermal ratings. The temporal correlations among the thermal ratings in 1 hour are strong. 2) The performance of single-period probabilistic predictions of thermal ratings can be improved by considering meteorological correlations. Compared with probabilistic predictions generated without considering meteorological correlations, the ACE and ASV are reduced by as much as 53% and 46%, respectively, and the CRPS is reduced by 44% on average. 3) The proposed JPDP-MPTR method can yield further improved

prediction results based on single-period probabilistic predictions by considering the temporal correlations among multiperiod thermal ratings. Compared with the results of single-period probabilistic predictions considering meteorological correlations, the ACE and ASV are further reduced by as much as 31% and 56%, respectively, and the CRPS is reduced by 45% on average.

Building on the present work, further analysis and refinement can be carried out to facilitate the application of the proposed method. First, the prediction time horizon considered in this paper (1 hour) was selected on the basis of an autocorrelative analysis of thermal ratings calculated based on meteorological data collected in the vicinity of a specific overhead conductor in a specific year. For overhead conductors in different locations and seasons, the autocorrelations among the thermal ratings under different retardation time windows may be different due to the influence of topography and seasonality; in such a case, the prediction time horizon should be reselected based on an autocorrelative analysis of corresponding historical thermal ratings. Moreover, the classic QR and copula-based joint distribution modeling methods were used in the proposed JPDP-MPTR method. We cannot rule out the possibility that some other methods may perform better than the QR and copula-based methods, thus having the ability to replace the QR and copula-based methods used in this paper. Therefore, future studies are needed to further improve the proposed JPDP-MPTR method by exploring and integrating other well-performed probabilistic prediction and correlation modeling methods. Finally, inspired by the studies on transient-state thermal rating prediction [36], the correlations among the four meteorological elements and the temporal correlations of meteorological elements can also be integrated into the probabilistic predictions of transient-state thermal ratings in future work.

REFERENCES

[1] A. Safdarian, M. Z. Degefa, M. Fotuhi-Firuzabad and M. Lehtonen, "Benefits of real-time monitoring to distribution systems: dynamic thermal rating," in IEEE Transactions on Smart Grid, vol. 6, no. 4, pp. 2023-2031, July 2015.

[2] S. Fan, G. He, X. Zhou and M. Cui, "Online Optimization for Networked Distributed Energy Resources with Time-Coupling Constraints," in IEEE Transactions on Smart Grid, doi: 10.1109/TSG.2020.3010866.

[3] N. Viafora, Morozovska K, Kazmi, S H H, et al, "Day-ahead dispatch optimization with dynamic thermal rating of transformers and overhead lines," Electric Power Systems Research, vol. 171, pp. 194-208, 2019.

[4] D. Douglass et al., "Real-Time overhead transmission-line monitoring for dynamic rating," in IEEE Transactions on Power Delivery, vol. 31, no. 3, pp. 921-927, June 2016, doi: 10.1109/TPWRD.2014.2383915.

[5] Bishnu P. Bhattarai, Jake P. Gentle, Timothy McJunkin, et.al, "Improvement of transmission line ampacity utilization by weather-based dynamic line rating," IEEE Trans. Power Del., vol. 33, no. 4, pp. 1853–1863, Aug. 2018.

[6] DAVISM W. A new thermal rating approach: the real-time thermal rating system for strategic overhead conductor transmission lines, part Ⅰ: General description and justification of the real-time thermal rating system[J]. IEEE Transactions on Power Apparatus and Systems, 1978, PAS-96(3):803-809.

[7] D. M. Greenwood and P. C. Taylor, "Investigating the impact of real-time thermal ratings on power network reliability," in IEEE Transactions on Power Systems, vol. 29, no. 5, pp. 2460-2468, Sept. 2014.

[8] D. M. Greenwood, G. L. Ingram and P. C. Taylor, "Applying wind simulations for planning and operation of real-time thermal ratings," in IEEE Transactions on Smart Grid, vol. 8, no. 2, pp. 537-547, March 2017.

[9] J. Zhan, C. Y. Chung and E. Demeter, "Time series modeling for dynamic thermal rating of overhead lines," in IEEE Transactions on Power Systems, vol. 32, no. 3, pp. 2172-2182, May 2017.

[10] C. J. Wallnerström, Y. Huang, and L. Söder, "Impact from dynamic line rating on wind power integration," IEEE Trans. Smart Grid, vol. 6, no. 1, pp. 343–350, Jan. 2015.

[11] R. Xiao, Y. Xiang, L. Wang and K. Xie, "Power system reliability evaluation incorporating dynamic thermal rating and network topology optimization," in

This article has been accepted for publication in a future issue of this journal, but has not been fully edited. Content may change prior to final publication. Citation information: DOI 10.1109/TPWRD.2020.3031833, IEEE Transactions on Power Delivery

> REPLACE THIS LINE WITH YOUR PAPER IDENTIFICATION NUMBER (DOUBLE-CLICK HERE TO EDIT) <   9

IEEE Transactions on Power Systems, vol. 33, no. 6, pp. 6000-6012, Nov. 2018.

[12] A. Bosisio, A. Berizzi, et al, "Improving DTR assessment by means of PCA applied to wind data," Electric Power Systems Research, vol. 172, pp. 193-200, 2019.

[13] Alvarez, D. L., da Silva, F. F., Mombello, E. E., Bak, C. L., & Rosero, J. A. (2018). Conductor temperature estimation and prediction at thermal transient state in dynamic line rating application. IEEE Transactions on Power Delivery, 33(5), 2236–2245.

[14] J. Jiang, Y. Liang, C. Chen, X. Zheng, C. Chuang and C. Wang, "On dispatching line ampacities of power grids using weather-based conductor temperature forecasts," in IEEE Transactions on Smart Grid, vol. 9, no. 1, pp. 406-415, Jan. 2018.

[15] S. Madadi, B. Mohammadi-ivatloo and S. Tohidi, "Dynamic line rating forecasting based on integrated factorized ornstein-uhlenbeck processes," IEEE Transactions on Power Delivery, pp. 1-1, 2019.

[16] Alexander W. Abbouda, Kenneth R. Fentonb, Jacob P. Lehmera, et.al. Coupling computational fluid dynamics with the high resolution rapid refresh model for forecasting dynamic line ratings [J]. Electric Power Systems Research, 2019, 170(7):326-337.

[17] T. Ringelb, P. Schäfer and A. Moser, "Probabilistic ampacity forecasting for overhead lines using weather forecast ensembles," Electrical Engineering, vol. 95, (2), pp. 99-107, 2013.

[18] F. Fan, K. Bell and D. Infield, "Probabilistic real-time thermal rating forecasting for overhead lines by conditionally heteroscedastic auto-regressive models," IEEE Transactions on Power Delivery, vol. 32, (4), pp. 1881-1890, 2017.

[19] J. L. Aznarte and N. Siebert, "Dynamic line rating using numerical weather predictions and machine learning: A case study," in IEEE Transactions on Power Delivery, vol. 32, no. 1, pp. 335-343, Feb. 2017.

[20] Romain Dupin, George Kariniotakis, Andrea Michiorri, Overhead lines dynamic line rating based on probabilistic day-ahead forecasting and risk assessment, International Journal of Electrical Power & Energy Systems, Volume 110, 2019.

[21] R. Dupin, A. Michiorri and G. Kariniotakis, "Optimal dynamic line rating forecasts selection based on ampacity probabilistic forecasting and network operators' risk aversion," in IEEE Transactions on Power Systems, vol. 34, no. 4, pp. 2836-2845, July 2019.

[22] M. Matus et al., "Identification of critical spans for monitoring systems in dynamic thermal rating," in IEEE Transactions on Power Delivery, vol. 27, no. 2, pp. 1002-1009, April 2012, doi: 10.1109/TPWRD.2012.2185254.

[23] J. Teh and I. Cotton, "Critical span identification model for dynamic thermal rating system placement," in IET Generation, Transmission & Distribution, vol. 9, no. 16, pp. 2644-2652, 3 12 2015, doi: 10.1049/iet-gtd.2015.0601.

[24] "IEEE Standard for Calculating the Current-Temperature Relationship of Bare Overhead Conductors," IEEE Std 738-2012 (Revision of IEEE Std 738-2006 - Incorporates IEEE Std 738-2012 Cor 1-2013)), pp. 1-72, 2013.

[25] K. V. Mardia, "Linear-circular correlation coefficients and rhythmometry," Biometrika, vol. 63, (2), pp. 403-405, 1976

[26] Cohen, J. (1988). Statistical power analysis for the behavioral sciences (2nd ed.). Hillsdale, NJ: Lawrence Erlbaum Associates.

[27] Deborah J. Rumsey. (2011) Statistics for dummies (2nd ed.). Hoboken, NJ. Wiley Publishing.

[28] F. Fan, K. Bell and D. Infield, "Probabilistic weather forecasting for dynamic line rating studies," 2016 Power Systems Computation Conference (PSCC), Genoa, 2016, pp. 1-7, doi: 10.1109/PSCC.2016.7540854.

[29] N. Zhang, C. Kang, C. Singh and Q. Xia, "Copula based dependent discrete convolution for power system uncertainty analysis," in IEEE Transactions on Power Systems, vol. 31, no. 6, pp. 5204-5205, Nov. 2016.

[30] J. A. Carnicero, M. C. Ausín and M. P. Wiper, "Non-parametric copulas for circular–linear and circular–circular data: an application to wind directions," Stochastic Environmental Research and Risk Assessment, vol. 27, (8), pp. 1991-2002, 2013.

[31] T. Bouezmarni, J. V. K. Rombouts and A. Taamouti, "Asymptotic properties of the Bernstein density copula estimator for α -mixing data," Journal of Multivariate Analysis, vol. 101, (1), pp. 1-10, 2010.

[32] Y. Wang, N. Zhang, C. Kang, M. Miao, R. Shi and Q. Xia, "An efficient approach to power system uncertainty analysis with high-dimensional dependencies," in IEEE Transactions on Power Systems, vol. 33, no. 3, pp. 2984-2994, May 2018.

[33] M. Cui, V. Krishnan, B. Hodge and J. Zhang, "A Copula-based conditional probabilistic forecast model for wind power ramps," in IEEE Transactions on Smart Grid, vol. 10, no. 4, pp. 3870-3882, July 2019.

[34] QIU Xiaoxia, LIU Cihua, WU Juan. The properties of maximum likelihood estimation of parameter on copula[J]. Mathematics in Economics, 2008, 25(2):210-215.

[35] A. Sancetta and S. Satchell, "The Bernstein copula and its applications to modeling and approximations of multivariate distributions," Econometric Theory, vol. 20, (3), pp. 535-562, 2004

[36] F. Fan, K. Bell and D. Infield, "Transient-state real-time thermal rating forecasting for overhead lines by an enhanced analytical method," Electric Power Systems Research, vol. 167, pp. 213-221, 2019.

Xu Jin was born in Jiangsu, China, in 1996. He is currently working toward the M.S. degree in electrical engineering at Shandong University, Jinan, China. His research interests include dynamic thermal rating estimation and forecast techniques.

Mengxia Wang (S'10-M'16) received the Ph.D. degree in electrical engineering from Shandong University, Jinan, China, in 2011. From July 2011 to July 2013, he conducted postdoctoral research with the Department of Electrical Engineering, Tsinghua University, Beijing, China. He is currently a Lecturer at Shandong University. His research interests are power system security analysis, optimal operation, and control.

Mingjian Cui (S'12-M'16-SM'18) received the B.S. and Ph.D. degrees from Wuhan University, Wuhan, Hubei, China, all in Electrical Engineering and Automation, in 2010 and 2015, respectively.

Currently, he is a Research Assistant Professor at Southern Methodist University, Dallas, Texas, USA. He was also a Visiting Scholar from 2014 to 2015 in the Transmission and Grid Integration Group at the National Renewable Energy Laboratory (NREL), Golden, Colorado, USA. His research interests include renewable energy, power system operation, power system cybersecurity, power system data analytics, and machine learning. He has authored/coauthored over 60 peer-reviewed publications. Dr. Cui serves as an Associate Editor for journals of IET SMART GRID, IEEE ACCESS, IEEE POWER ENGINEERING LETTERS, and IEEE OPEN ACCESS JOURNAL OF POWER AND ENERGY (OAJPE). He is also the Best Reviewer of IEEE TRANS. SMART GRID for 2018 and IEEE TRANS. SUSTAINABLE ENERGY for 2019.

Hua Sun received the M.S. degree from the School of Electrical Engineering at Shandong University, Jinan 250061, China, in 2005. She is currently a lecturer with Technician Department, Shandong Labour Vocational and Technical College, Jinan, 250022, China. Her research interest includes power system stability and power system operation.

Ming Yang (M'09-SM'18) received the B.Eng. and Ph.D. degrees in electrical engineering from Shandong University, Jinan, China, in 2003 and 2009, respectively. He was an exchange Ph.D. student with the Energy System Research Center. The University of Texas at Arlington, Arlington, TX, USA, from October 2006 to October 2007. He conducted Postdoctoral research with the School of Mathematics of Shandong University from July 2009 to 2011.From November 2015 to October 2016, he was a Visiting Scholar with the Energy Systems Division, Argonne National Laboratory, Argonne, IL, USA. He is currently a Professor with the Shandong University and an Associate Editor of the IEEE Transactions on Industry Applications. His research interests include power system optimal operation and control.